energies

MDPI

Article

Dynamic Propagation and Shear Stress Disturbance of Multiple Hydraulic Fractures: Numerical Cases Study via Multi-Well Hydrofracturing Model with Varying Adjacent Spacings

Yongliang Wang [1,2,*] and Nana Liu [1]

[1] School of Mechanics and Civil Engineering, China University of Mining and Technology, Beijing 100083, China; liunana@cumtb.edu.cn
[2] State Key Laboratory of Coal Resources and Safe Mining, China University of Mining and Technology, Beijing 100083, China
* Correspondence: wangyl@cumtb.edu.cn

Abstract: Multi-well hydrofracturing is an important technology for forming complex fracture networks and increasing reservoir permeability. The distribution and design of horizontal wells affect fracture propagation; however, it is still unclear how the spacing between adjacent wells leads to fracture propagation, deflection and connection. In this study, the thermal-hydro-mechanical coupling effect in the hydrofracturing process is comprehensively considered and a multi-well hydrofracturing model based on the finite element–discrete element method is established. Using typical cases, the unstable propagation of hydraulic fractures in multiple horizontal wells under varying adjacent well spacings is studied. Combined with the shear stress shadow caused by in situ stress disturbed by fracture tip propagation, quantitative indexes (such as length, volume, deflection and unstable propagation behaviors of hydrofracturing fracture networks) are analyzed. The results show that the shear stress disturbance caused by multiple hydraulic fractures is a significant factor for multi-well hydrofracturing. Reducing well spacing will increase the stress shadow area and aggravate the mutual disturbance and deflection between fractures. The results of quantitative analysis show that the total length of hydraulic fractures decreases with the decrease of well spacing, and the total volume of hydraulic fractures increases with the decrease of well spacing. The results of unstable propagation and stress evolution of hydraulic fracture networks considering thermal-hydro-mechanical coupling obtained in this study can provide useful guidance for the valuation and design of hydrofracturing fracture networks in deep unconventional oil and gas reservoirs.

Keywords: multi-well hydrofracturing; unstable fracture propagation; shear stress disturbance; well spacing; thermal-hydro-mechanical coupling

Citation: Wang, Y.; Liu, N. Dynamic Propagation and Shear Stress Disturbance of Multiple Hydraulic Fractures: Numerical Cases Study via Multi-Well Hydrofracturing Model with Varying Adjacent Spacings. *Energies* **2022**, *15*, 4621. https://doi.org/10.3390/en15134621

Academic Editor: Kamy Sepehrnoori

Received: 25 April 2022
Accepted: 1 June 2022
Published: 24 June 2022

1. Introduction

The complexity of hydraulic fracture networks is the key to increasing unconventional oil and gas production [1]. Multi-well hydrofracturing is an important technology for forming complex fracture networks and increasing reservoir permeability. Compared with single-well hydrofracturing, the interaction between fractures in multi-well hydrofracturing is more complex. Figure 1 shows unstable dynamic propagation and deflection of multiple hydraulic fractures in multi-well hydrofracturing in tight reservoirs, in which the dynamic propagation of multiple hydraulic fractures is simultaneously affected by the adjacent perforation clusters (*a*: perforation cluster spacing) and adjacent wells (*b*: well spacing), resulting in a more complex fracture network. The hydrofracturing-induced stress field places pressure on the surrounding rock, altering the initiation pressure in the subsequent perforation, the in situ stress field and the propagation direction of hydraulic fractures [2–8]. The hydrofracturing-induced stress field not only can promote fracture propagation and form a more complex fracture network [9–12], but can also inhibit the

growth of local fractures [6,13–15], which are not conducive to controlling the fracture propagation process and increasing unconventional oil and gas production [16–18]. It is vital to understand the relationship between the geometric distributions of multiple wells and the induced stress field and fracture propagation, so as to evaluate and optimize the hydraulic fracturing process.

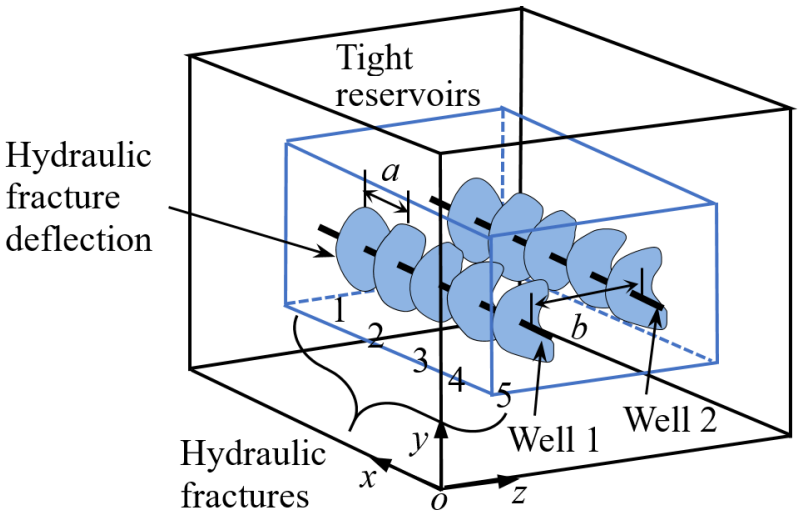

Figure 1. Schematic of unstable dynamic propagation and deflection of multiple hydraulic fractures in multi-well hydrofracturing (*a*: perforation cluster spacing, *b*: well spacing).

The spacing of perforation clusters, fracturing sequence and well spacing are considered to be the dominant factors causing unstable propagation of parallel fractures in different extents in multi-well hydrofracturing [19–22]. When two adjacent horizontal wells are designed, the hydraulic fractures in the subsequent well propagate away from the previous well [22]. Narrow adjacent well spacing may result in intersecting stimulation reservoir volumes, causing competition behaviors between wells and affecting fracture propagation and oil and gas production [23,24]. Well spacing should be carefully selected to avoid the connection of fracture tips in adjacent horizontal wells; some studies have carried out analysis from the perspective of the hydrofracturing-induced stress field evolution. A small well spacing may create drastic stress disturbances between wells, resulting in connections of hydraulic fractures from adjacent wells in a short duration time of hydrofracturing, which inevitably reduces fracture complexity in the far field. On the other hand, if the well spacing is too large, the natural fracture between the two wells cannot be reactivated [25–27]. The spacing between adjacent wells can be optimized by using the variation of induced stress field evolution and disturbance in the hydrofracturing process. The simulation and evaluation results of the fracture path in the simultaneous fracturing of two horizontal wells show that when the well spacing exceeds 60 m, it can effectively alleviate the stress disturbance and improve the fracturing effects [27].

The stress shadow effect between multiple wells affects the dynamic propagation of fracture network; hence, it is critical to determine the internal mechanisms of the stress shadow effect in multi-well hydrofracturing to optimize the fracturing schemes [21,28]. The stress shadow effect depends on fracture height, mechanical properties (i.e., Young's modulus and Poisson's ratio), cluster spacing and well spacing [29–31]. When multiple horizontal wells are adjacent to each other, the stress shadows induced by perforation clusters will affect the fracture propagation patterns in each well [24]. Increasing well spacing can effectively alleviate the stress shadow effect [27,28]. However, it is still unclear how the spacings between adjacent wells lead to fracture propagation, deflection and connection, and the quantitative relationship between the induced stress field and fracture propagation is not well understood.

In order to further investigate the effect of adjacent well spacing on dynamic propagation and shear stress disturbance in multi-well hydrofracturing, the main contents of this paper are investigated as follows. Section 2 introduces the combined finite element–discrete element method considering thermal-hydro-mechanical coupling. Section 3 introduces the numerical models and cases of multiple horizontal wells, including the geometric model, finite element model, conditions and parameters setting. Section 4 introduces the results and discussions. Section 5 summarizes the conclusions of this study and prospects for future research.

2. Combined Finite Element–Discrete Element Method Considering Thermal-Hydro-Mechanical Coupling

In the hydrofracturing of the reservoir rock, the thermal field, hydraulic field and mechanical field form a mutual coupling process [32,33]. The main mechanism of the coupling process is shown in Figure 2 [34]. Through the transfer between solid stress, fluid pressure, heat and fracture networks, the thermal-hydro-mechanical coupling and fracture network mechanisms are introduced [35].

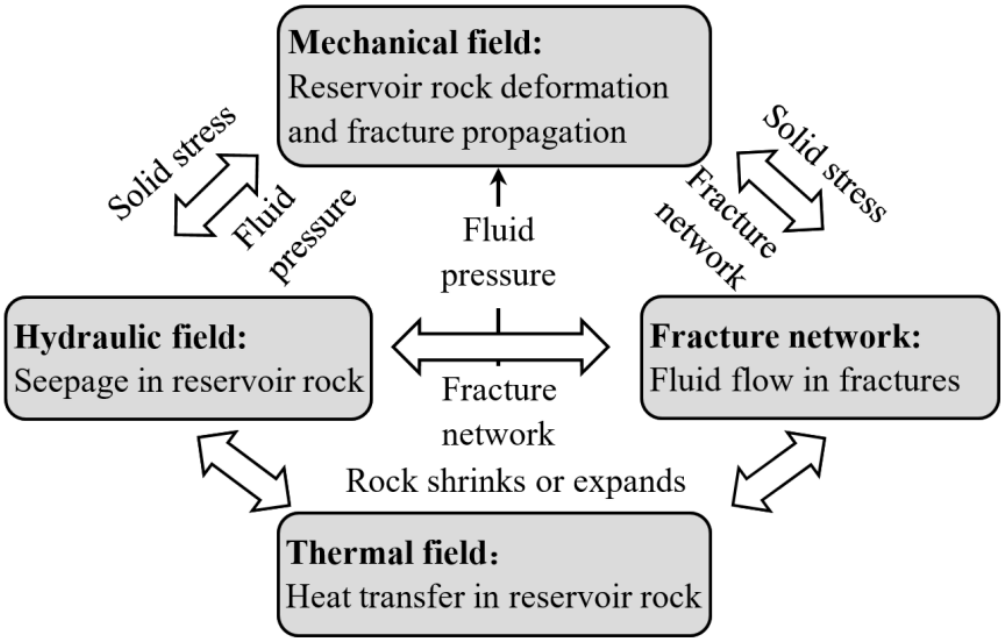

Figure 2. Thermal-hydraulic-mechanical coupling and fracture propagation mechanisms.

The staggered coupling scheme is adopted in this study. In hydraulic field, under the current deformation and fracture network of solid rock, the fluid pressures in the pore media of the rock matrix and fractures are computed, and the fluid pressures are transmitted to the rock matrix. In the thermal field, the heat transfer in the pore media of the rock matrix and fracture fluid are computed through the governing equation of the current time, and the heat is transmitted to the rock matrix where it induces thermal stresses. In the mechanical field, the solid deformation and stresses in the pore media of the rock matrix are computed. Furthermore, by introducing the thermal stresses, the final effective stresses can be obtained. Based on the stress states of each finite element, the fracture criterion is used to judge whether the fractures initiate or propagate. In this study, the fracture criterion considering damage evolution is used to simulate the propagation of hydraulic fractures, and the tensile strength σ_t and fracture energy G_f are involved, the details of which can be found in the related reference [36].

The governing equations for solid deformation, fluid flow and heat transfer are as follows:

(1) Solid deformation

The governing equation of rock mass matrix deformation is [37]:

$$\mathbf{L}^{\mathrm{T}}(\boldsymbol{\sigma}^{'} - \boldsymbol{\alpha}\mathbf{m}p_l) + \boldsymbol{\rho}_B\mathbf{g} = \mathbf{0} \tag{1}$$

where $\mathbf{L}$ is the differential operator, $\boldsymbol{\sigma}^{'}$ is the effective stress tensor with $\boldsymbol{\sigma}^{'} = \boldsymbol{\sigma} + \alpha\mathbf{I}p$, α is Biot's coefficient, $\boldsymbol{\sigma}$ is the stress tensor of the rock matrix, $\mathbf{m}$ denotes the identity tensor, p_l is the pore fluid pressure of the rock mass, ρ_B is the saturated bulk density of the rock mass and $\mathbf{g}$ is the gravity vector. The inertia term is not concluded and the quasi-static state is considered, which is a basis for detecting the deformation and behavior of rock mass in this study.

(2) Fluid flow

The governing equation of seepage in rock matrix is:

$$\mathrm{div}\left[\frac{k}{\mu_l}(\nabla p_l - \rho_l\mathbf{g})\right] = \left(\frac{\varphi}{K_l} + \frac{\alpha - \varphi}{K_s}\right)\frac{\mathrm{d}p_l}{\mathrm{d}t} + \alpha\frac{\mathrm{d}\varepsilon_v}{\mathrm{d}t} \tag{2}$$

where k is the intrinsic permeability of rock mass, μ_l is the viscosity of the pore liquid, ρ_l is the pore liquid density, φ is the porosity of porous medium, K_l is the pore fluid stiffness, K_s is the solid skeleton stiffness, ε_v is the volumetric strain of rock mass pore structure and t is the current moment.

The governing equation of fluid flow in the fracture is:

$$\frac{\partial}{\partial x}\left[\frac{k^{fr}}{\mu_n}\left(\nabla p_n - \rho_{fn}\mathbf{g}\right)\right] = S^{fr}\frac{\mathrm{d}p_n}{\mathrm{d}t} + \alpha\left(\Delta\dot{e}_\varepsilon\right) \tag{3}$$

where k^{fr} is the fracture intrinsic permeability, μ_n is the viscosity of the fracturing fluid, p_n is fluid pressure in the fracture, ρ_{fn} is fluid density in the fracture, S^{fr} is the parameter describing rock mass compressibility under fluid action and $\frac{\mathrm{d}\Delta\dot{e}_\varepsilon}{\mathrm{d}t}$ is the strain rate. According to the plate theory of fluid, the permeability of the fluid in the fracture is:

$$k^{fr} = \frac{e^2}{12} \tag{4}$$

where e is the fracture width. The fracture propagation width (aperture) can be obtained through the deformation of the rock surrounding the fracture. In the process of hydrofracturing, the fluid drives the fracture propagation, which will form the opening of the fracture width (aperture) and the fracture closure. This closure process can be obtained according to the deformation (displacement) of the surrounding rock around the fracture. The opening and closing of the fracture will lead to the change of the internal fluid storage volume, resulting in the variation of permeability and compressibility of the fluid in the hydraulic fracture, and the hydrodynamic behaviors of fluid will simultaneously change. The parameters for compressibility are expressed as:

$$S^{fr} = \left(\frac{1}{e}\right)\left[\left(\frac{1}{K_n^{fr}}\right) + \left(\frac{e}{K_f^{fr}}\right)\right] \tag{5}$$

where K_n^{fr} is the normal stiffness of the fracture and K_f^{fr} is the bulk modulus of the fracturing fluid. Seepage in the rock matrix and seepage in the fracture are distinguished according to the material domains, and the corresponding governing Equations (2) and (3) are used.

(3) Heat transfer

The governing equation of heat transfer between the rock matrix and fracturing fluids is:

$$\operatorname{div}\left[k_b \nabla T_f\right] = \rho_b c_b \frac{\partial T_f}{\partial t} + \rho_f c_f \mathbf{q}_f \nabla T_f \tag{6}$$

where k_b is the thermal conductivity coefficient, T_f is fluid temperature, ρ_b is volume density, c_b is the specific heat coefficient, ρ_f is fluid density, c_f is the specific heat coefficient of fluid, and $\mathbf{q}_f$ is Darcy fluid flux.

Heat transfer between the finite element nodes in formation and network is shown in Figure 3.

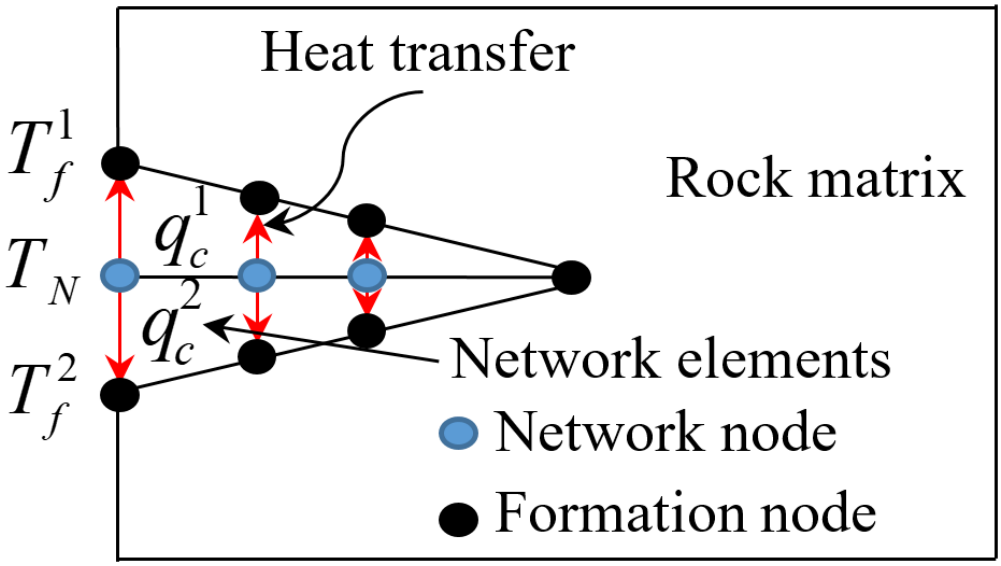

Figure 3. Heat transfer between finite element nodes in formation and network.

The heat transfer from the fracture network element from the fluid in the fracture zone to the rock matrix is as follows [38]:

$$q_c^1 = \alpha_c(T_N)\left(T_N - T_f^1\right) \tag{7}$$

$$q_c^2 = \alpha_c(T_N)\left(T_N - T_f^2\right) \tag{8}$$

where q_c^1 and q_c^2 are the contact heat flow between the network and formation nodes, respectively, T_N is the temperature value of the node within the fracture and α_c is the contact thermal conductivity; T_f^1 and T_f^2 are the corresponding formation node temperatures.

Heat transfer through a reservoir rock can cause stress changes owing to rock shrinkage or expansion, and the volume change depends on the linear thermal coefficient of expansion:

$$\frac{\Delta V}{V} = \alpha_T \Delta T \tag{9}$$

where V is the initial volume, ΔV is the incremental volume, ΔT is the incremental temperature and α_T is the linear thermal expansion coefficient of the rock matrix. The variation of volume induced by temperature field may lead to the variation of stain (thermal strain) of the rock matrix. By means of the relationship between strain and stress (e.g., the constitutive relation), the temperature strain will produce the thermal stress.

In the technical aspects of the numerical solution, some detailed content, such as numerical implementation and orders of finite elements, was omitted to avoid redundancy. In this study, the combined finite element–discrete element method is used to simulate the hydraulic fracturing process. The governing equations are discretized using the finite

element method. The order of the finite elements is linear. The computation accuracy of these linear elements will be insufficient compared with higher-order elements; however, the adaptive mesh refinement technology used in this study improves the solution accuracy. The nonlinear ordinary differential equations can be obtained by numerical discretization according to the finite element method. These nonlinear equations are computed by iterative methods, e.g., the Newton–Raphson iteration method.

3. Numerical Models and Cases of Multiple Horizontal Wells

In this paper, a numerical model of multi-well multistage fracturing in deep tight reservoirs is established, as shown in Figure 4. Three horizontal wells (denoted as Well 1, Well 2 and Well 3) are set in this model, and five perforation clusters (numbers are 1–5 in sequence) are set for each well. There are two geometric variables in the model; a is the perforation cluster spacing and b is the well spacing. Figure 5 shows the initial mesh refinement of the finite element model; an initial dense mesh is used around local perforation domains to guarantee a reliable fracture propagation path in the initial stage. For the boundary conditions of solid field, the treatment technique of this model is to use the displacement boundary conditions (Dirichlet boundary conditions) to fix the displacements on the six surfaces of the model and impose in situ stresses at each node in the finite element model, so as to form the in situ stress field at the initial stage.

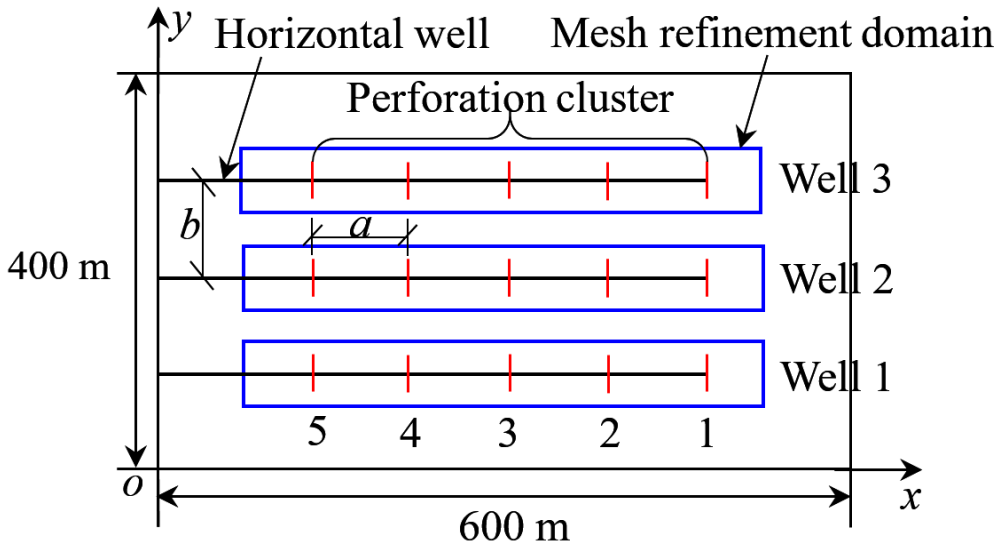

Figure 4. Geometric model of multi-well multistage fracturing.

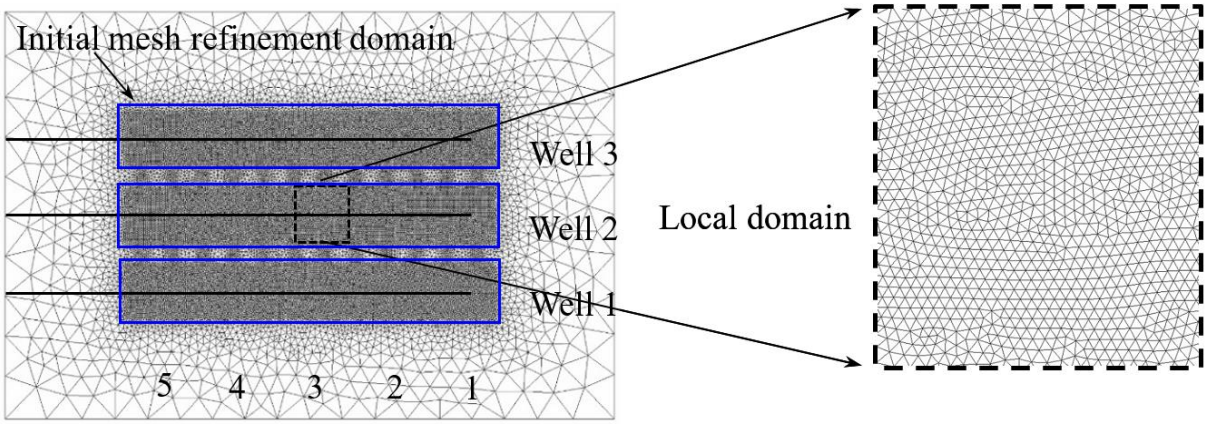

Figure 5. Initial mesh refinement of the finite element model.

In the study of unstable propagation of fractures at different well spacing, the perforation cluster spacing a is 75 m and the well spacings b are 100 m, 75 m and 50 m. The numerical cases of different well spacings are shown in Table 1; the perforation clusters on each well use sequential fracturing (1→2→3→4→5), the temperature of the fracturing fluid is set to 20 °C and the rock matrix temperature is set to 60 °C. The basic physical parameters of the model are set as shown in Table 2, which were tested on the tight rock samples in the Shengli Oilfield in Shandong Province in China.

Table 1. Numerical cases of different well spacings.

Case	a (m)	b (m)	Fracturing Fluid Temperature (°C)	Rock Matrix Temperature (°C)
I	75	100	20	60
II	75	75	20	60
III	75	50	20	60

Table 2. Basic physical parameters of the numerical model.

Parameters	Value
Horizontal minimum in-situ stress (x-direction) S_h(MPa)	40
Horizontal maximum in-situ stress (y-direction) S_H(MPa)	44
Fluid injection rate Q (m^3/s)	0.5
Pore pressure p_l (MPa)	10
Biot's coefficient α	0.75
Elastic modulus E (GPa)	31
Poisson's ratio ν	0.22
Penetration k (nD)	50
Porosity φ	0.05
Kinematic viscosity coefficient $\mu_n(Pa \cdot s)$	1.67×10^{-3}
Fracture fluid bulk modulus K_f^{fr} (MPa)	2000
Tensile strength σ_t(MPa)	5.26
Fracture energy $G_f(\mathrm{N} \cdot \mathrm{m})$	165

4. Results and Discussions

4.1. Thermal Diffusion in Fracture Propagation Process

The thermal diffusion behaviors between het rock matrix (initial temperature is 60 °C) and fracturing fluid (initial temperature is 20 °C) in the propagation process of hydrofracturing is analyzed below. Figure 6 shows the temperature evolution around hydraulic fractures in multi-well hydrofracturing. From Figure 6a–c, with the propagation of fractures in perforation 1 in Well 1, the thermal diffusion occurs between the perforation cluster and surrounding rock matrix due to the existence of a temperature gradient. The fracturing fluid gradually rises to the temperature of the formation during fracture propagation. Figure 6d is the temperature field distribution of the three wells in the final stage, and thermal diffusion occurs near each perforation; with the termination of fracturing fluid injection in the perforation cluster, the thermal diffusion between the perforation cluster and the surrounding rock matrix weakens.

4.2. Fracture Network Propagation and Shear Stress Shadows

4.2.1. Case I: Well Spacing b = 100 m

In order to analyze the final fracture network morphology and deformation in multi-well fracturing, Figure 7 shows the distribution of hydraulic fractures when the well spacing is 100 m, and the displacement (m) in the x direction is provided to detect the deformation in the reservoir. The fractures 3, 4 and 5 of Well 1 are affected by the previous fractures 1 and 2, and deflect away from the previous fractures, which is identical to the multistage hydrofracturing in a single horizontal well [39]. Due to the influence of Well 1 on the in situ environment of the reservoir, fractures 1 and 2 of Well 2 penetrate through Well 1, and

fractures 3, 4 and 5 of Well 2 deflected in different extents from Well 1; due to the influence of Well 1 and Well 2 on the in situ environment of the reservoir, fractures 1 and 2 in Well 3 are connected with Well 1, and fractures 3, 4 and 5 are deflected dramatically away from Well 2. Meanwhile, both sides of the stratum are deformed to the left and right, respectively, which is caused by fracturing fluid injected into the reservoir.

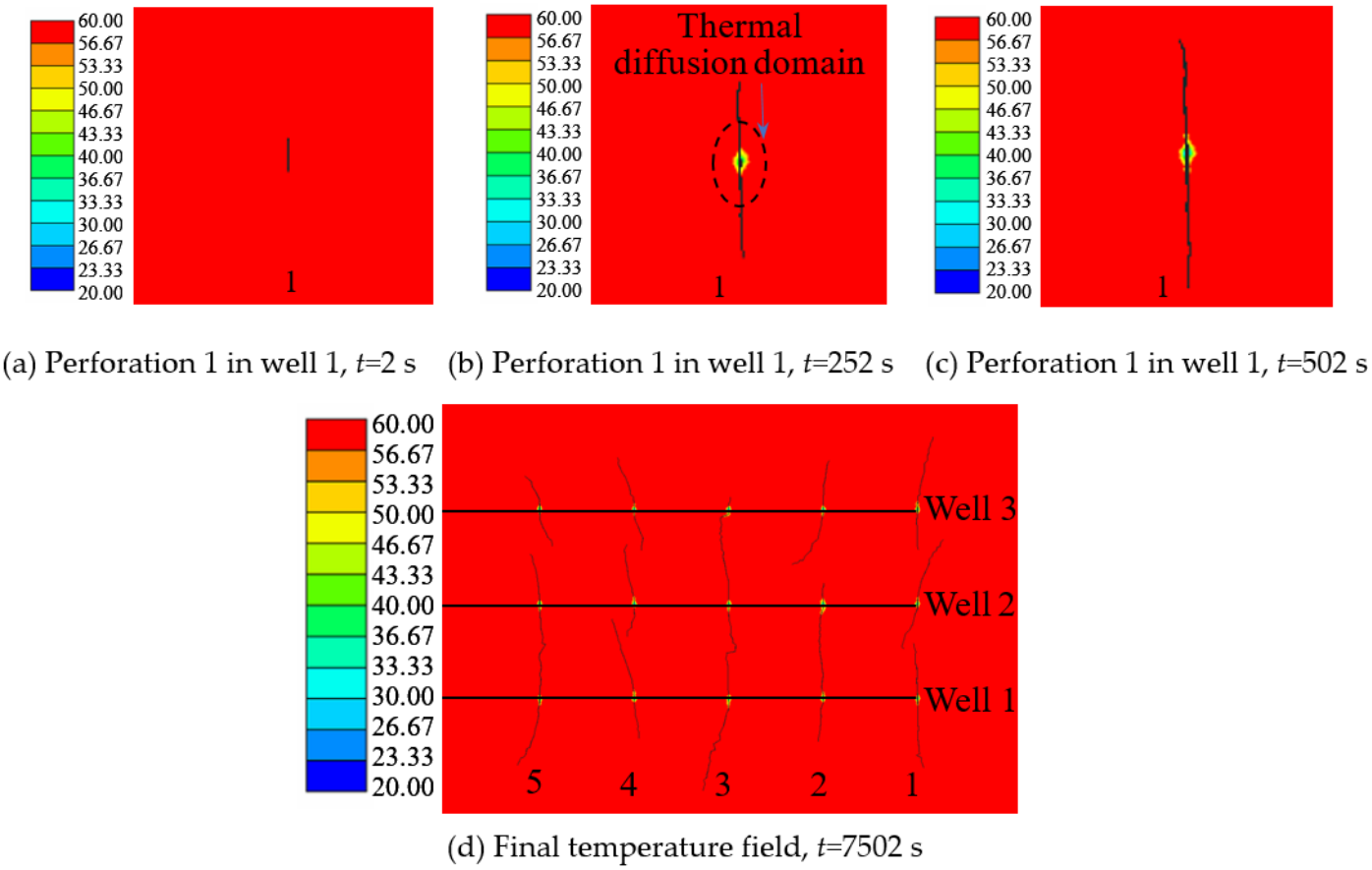

(a) Perforation 1 in well 1, t=2 s (b) Perforation 1 in well 1, t=252 s (c) Perforation 1 in well 1, t=502 s

(d) Final temperature field, t=7502 s

Figure 6. Temperature evolution around hydraulic fractures in multi-well hydrofracturing.

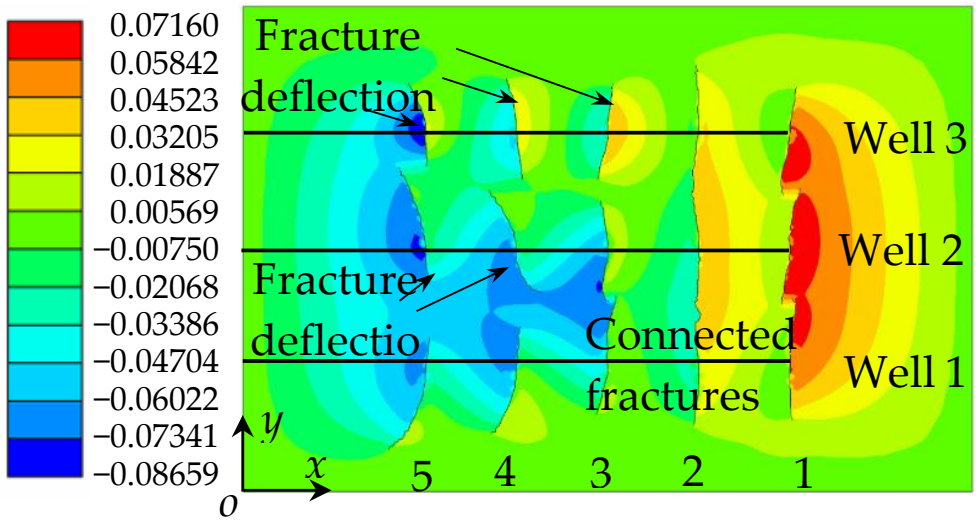

Figure 7. Final fracture network morphology and deformation in multi-well fracturing; b = 100 m.

Figure 8 shows the evolution of shear stress τ_{xy} in sequential fracturing at 100 m well spacing, at t = 2502 s, t = 5002 s and t = 7502 s. Figure 8a shows the shear stress results of Well 1 after the sequential fracturing is completed. The superposition and reduction of positive and negative shear stress fields around fracture tips result in unequal stresses on both sides of these fracture tips, and the fracture deflects towards the high stress domain. In Figure 8b, in the local areas of the two adjacent wells, the superposition and reduction of shear stresses occur (e.g., fracture 5 in Wells 1 and 2); and these stress disturbances deflect the fractures. Meanwhile, the stress area (indicated by dashed line) of the disturbed formation in Well 2covers the positions where the fractures in Well 3 will propagate, which is the stress shadow area between multiple wells. In Figure 8c, fractures 1 and 2 in Well 3 and Well 2 are penetrated and connected, and the deflection of fractures 3, 4, and 5 occurs due to the influence of stress shadows.

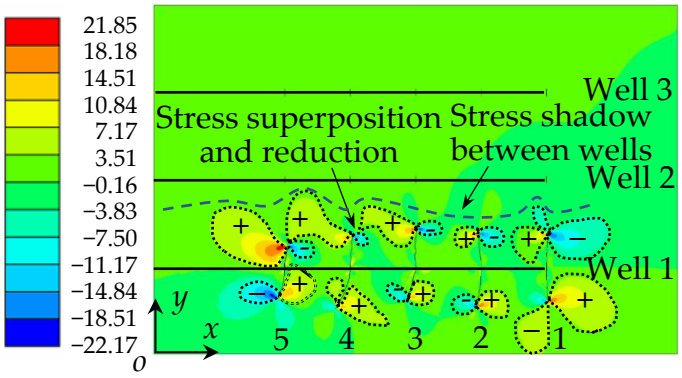

(**a**) t = 2502 s

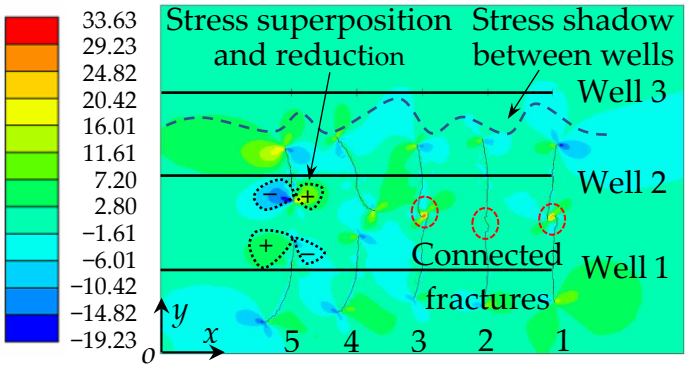

(**b**) t = 5002 s

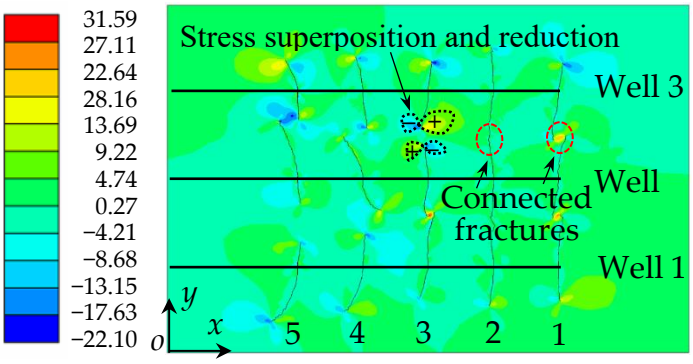

(**c**) t = 7502 s

Figure 8. Evolution of shear stress τ_{xy} (Mpa) in sequential fracturing at 100 m well spacing.

4.2.2. Case II: Well Spacing b = 75 m

Figure 9 shows the final fracture network morphology and deformation in multi-well fracturing when the well spacing is 75 m. After the propagation of five fractures in Well 1, due to the influence of Well 1 on the in situ environment of the reservoir, each fracture in Well 2 is connected with Well 1 and the fractures are deflected to varying away from Well 1; the fractures in Well 3 are deflected greatly away from Well 2. Compared with the results with 100 m well spacing, smaller well spacing of 75 m makes subsequent fractures easier to deflect and adjacent fractures easier to connect together.

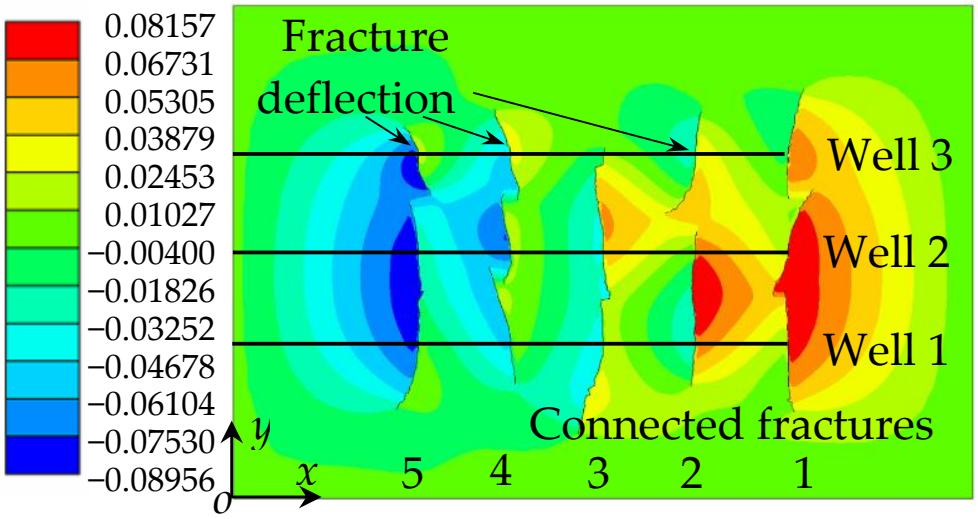

Figure 9. Final fracture network morphology and deformation in multi-well fracturing; b = 75 m.

Figure 10 shows the evolution of shear stress τ_{xy} in sequential fracturing at 75 m well spacing at t = 2502 s, t = 5002 s, t = 7502 s. Figure 10a shows the shear stress results of Well 1 after the sequential fracturing is completed. The superposition and reduction of positive and negative shear stress fields around fracture tips result in unequal stresses on both sides of these fracture tips, and the fracture deflects toward the high stress domain, which is similar to Figure 8a. In Figure 10b, in the local areas of the two adjacent wells, the superposition and reduction of shear stresses occur (e.g., fracture 5 in Wells 1 and 2); and these stress disturbances deflect the fractures. Meanwhile, the stress area (indicated by dashed line) of the disturbed formation in Well 2 covers the positions where the fractures in Well 3 will propagate, which is the stress shadow area between multiple wells. In Figure 10c, fracture 3 in Well 3 and Well 2 is penetrated and connected, and the deflection of fractures 1, 2, 4, and 5 occurs due to the influence of stress shadows.

4.2.3. Case III: Well Spacing b = 50 m

Figure 11 shows the final fracture network morphology and deformation in multi-well fracturing when the well spacing is 50 m. After the propagation of five fractures in Well 1, the fractures in Wells 1 and 2 are connected, causing the narrow well spacing. In Well 3, except for fracture 3 connecting with the adjacent fracture, the other fractures are deflected to varying extents by the fractures in Well 2. Compared with the results in well spacings of 100 m and 75 m, continuing to reduce well spacing leads to more fracture connection and penetration.

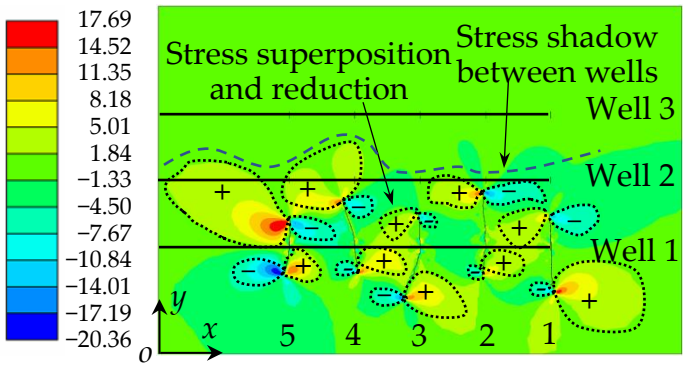

(**a**) t = 2502 s

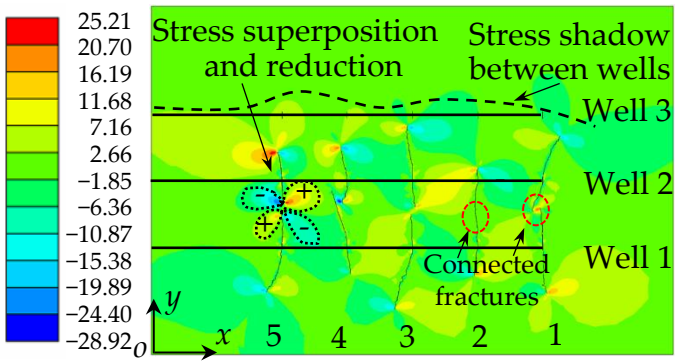

(**b**) t = 5002 s

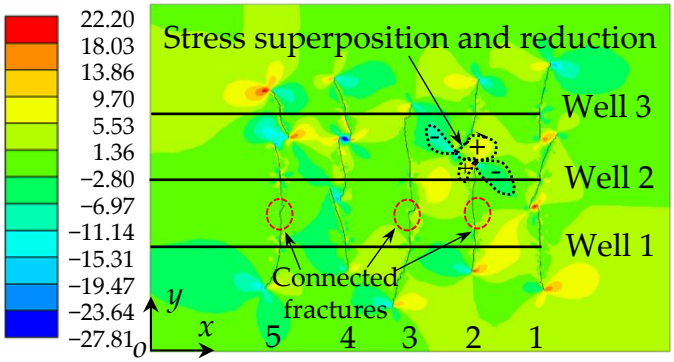

(**c**) t = 7502 s

Figure 10. Evolution of shear stress τ_{xy} (Mpa) in sequential fracturing at 75 m well spacing.

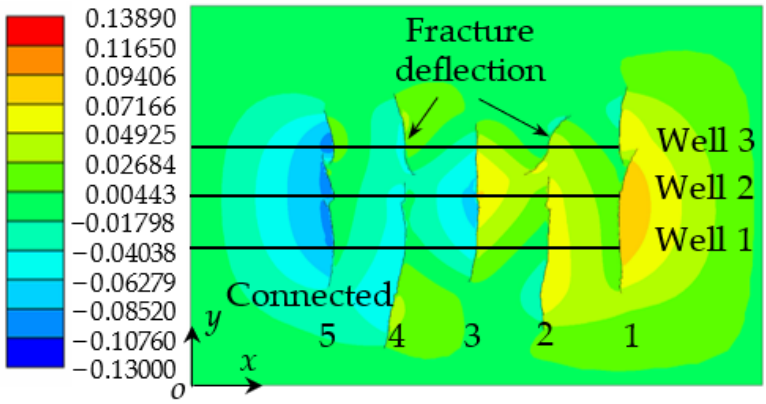

Figure 11. Final fracture network morphology and deformation in multi-well fracturing; b = 50 m.

Figure 12 shows the evolution of shear stress τ_{xy} in sequential fracturing at 50 m well spacing, at t = 2502 s, t = 5002 s and t = 7502 s. Figure 12a shows the shear stress results of Well 1 after the sequential fracturing is completed. The superposition and reduction of positive and negative shear stress fields around fracture tips result in unequal stresses on both sides of these fracture tips, and the fracture deflects toward the high stress domain. In Figure 12b, in the local areas of the two adjacent wells, the superposition and reduction of shear stresses occur (e.g., fracture 3 in Wells 1 and 2); and these stress disturbances deflect the fractures. Meanwhile, the stress area (indicated by dashed line) of the disturbed formation in Well 2 cover the positions where the fractures in Well 3 will propagate, which is the stress shadow area between multiple wells. In Figure 12c, the fractures 1, 2, 3 and 5 in Well 3 and Well 2 are penetrated and connected, and the deflection of fracture 4 occurs due to the influence of stress shadows.

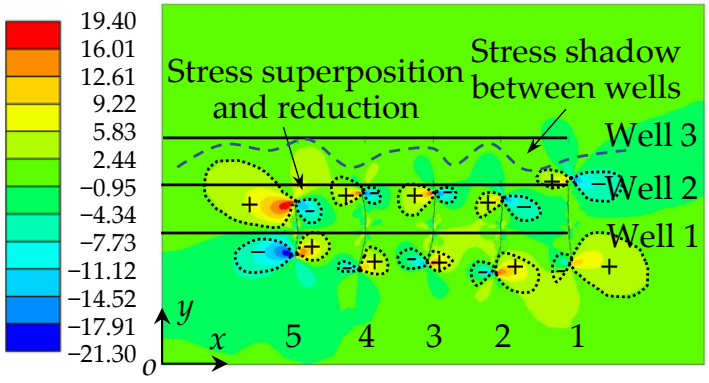

(**a**) t = 2502 s

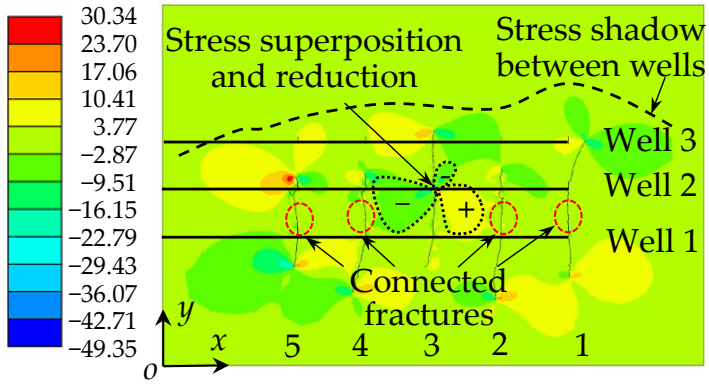

(**b**) t = 5002 s

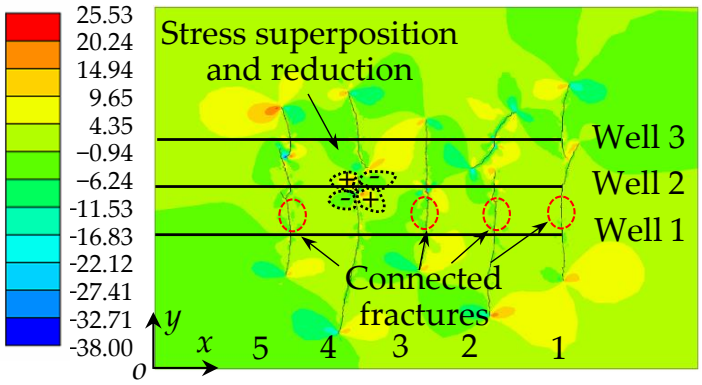

(**c**) t = 7502 s

Figure 12. Evolution of shear stress τ_{xy} (Mpa) in sequential fracturing at 50 m well spacing.

Comparing the fracture network propagation and shear stress evolution of the above different well spacings, with the decrease of well spacing, the stress shadow area between adjacent wells increases, and the stress superposition and reduction increase. The fracture propagation is inhibited, the propagation length of connected fractures decreases and the deflection extent of the deflection fracture increases. The stress field disturbance generated by the fracture propagation of the previous horizontal well gradually increases the inhibitory effect on the fracture propagation of the subsequent horizontal well.

4.3. Quantitative Analysis of Fracture Length and Volume

In order to quantitatively analyze the propagation behaviors of the fracture network in the multi-well hydrofracturing model with varying adjacent spacings, the fracture length and volume of fracture network for different stages and well spacings are derived as shown in Table 3. In the computation process, the discrete element method is used to analyze whether the element meets the fracture criterion to initiate and propagate. The fracture length can be found through the fracture propagation of the statistical elements. In addition, the fracture propagation width (aperture) can be obtained through the deformation of rock surrounding the fracture, and the fracture volume can be obtained by multiplying the fracture length and width (and the unit thickness of the model). With the injection of fracturing fluid, the total length and volume of the fractures increase. For the convenience of comparison and analysis, Figures 13 and 14 shows the curves of the length and volume of the fracture network under different well spacings with time. The length of hydraulic fractures from the initial stage shows a decreasing trend with reduced well spacing b (b = 100 m→75 m→50 m); the reason is that the reduction of well spacing intensifies the stress shadow between fractures. On the other hand, the fracture volume from the initial stage shows an increasing trend with reduced well spacing b; the reason is that the fractures that do not easily propagate forward may hold more fracturing fluid. The final total fracture length is the largest when the well spacing is 100 m, and the final total fracture length is the smallest when the well spacing is 50 m.

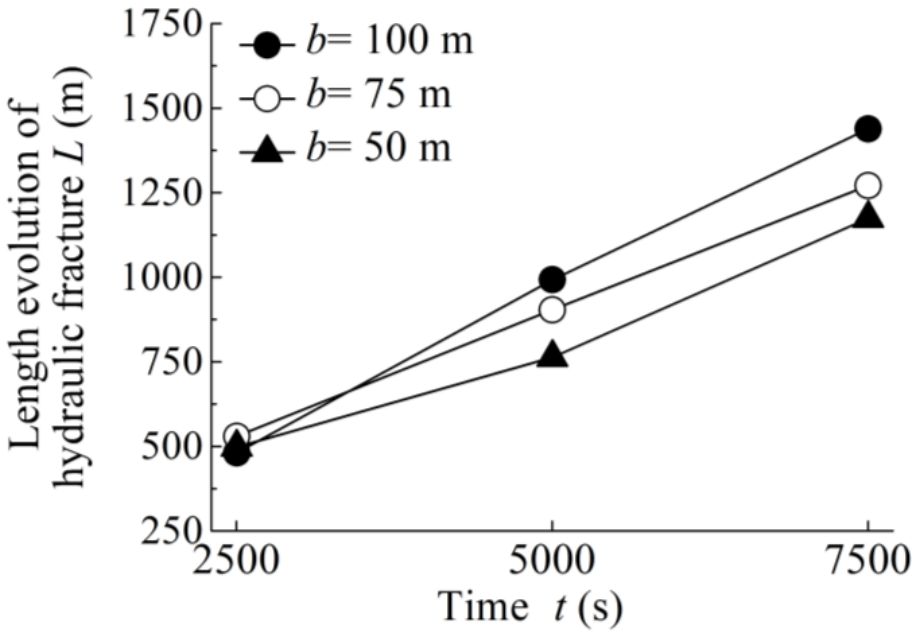

Figure 13. Length evolution of hydraulic fracture for different stages and well spacings.

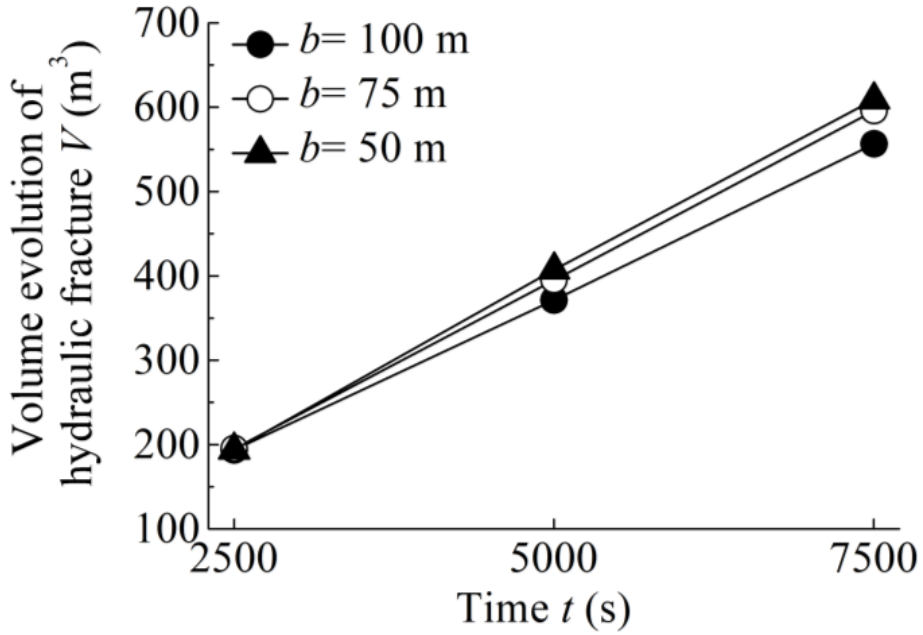

Figure 14. Volume evolution of hydraulic fracture for different stages and well spacings.

Table 3. Fracture length and volume of fracture network for different stages and well spacings.

b (m)	Time t (s)	Fracture Length L (m)	Fracture Volume V (m^3)
100	Stage 1 (t = 2502 s)	480.76	193.58
75		529.62	195.12
50		498.00	193.73
100	Stage 2 (t = 5002 s)	992.45	371.39
75		903.94	395.10
50		763.11	407.22
100	Stage 3 (t = 7502 s)	1438.69	556.38
75		1271.25	595.70
50		1174.75	608.84

The linear influence of well spacing on the propagation length and volume of the fracture network is reflected above, which can provide a reference for the evaluation of fracture networks in multi-well hydrofracturing. However, this evaluation alone is not enough; in the future, it is necessary to further investigate the influence of the smaller spacing of multiple wells (the linear relationship may no longer be valid). In addition, the impact of fracture distribution on oil and gas production should also be evaluated, because under the same fracture length and volume, different distribution forms of fracture networks will produce different oil and gas production and connect with different reservoir areas. These are some in-depth research topics to be carried out in the near future.

5. Conclusions

In this study, a multi-well hydrofracturing model is used to simulate and analyze the hydrofracturing process of multiple horizontal wells with different well spacings. The unstable propagation and stress evolution of fracture networks considering thermal-hydro-mechanical coupling are studied through the disturbed shear stress field and fracture length and volume. Some conclusions can be summarized:

1. In multi-well hydrofracturing, the stress around the fracture interferes with adjacent fractures in adjacent wells. The shear stress fields around the fractures of horizontal wells are superimposed, and the fractures are deflected to the side with the larger shear stress; multi-well hydrofracturing will lead to fracture connectivity between wells;

2. Varying well spacing will affect the unstable propagation of hydraulic fractures. With the decrease of well spacing, the disturbance of the stress field and the stress shadow area between wells gradually increase, the number of connected fractures also increases, the propagation length of the connected fractures gradually decreases and the unconnected fractures deflect. The degree of deflection increases and well spacing becomes an important factor affecting fracture propagation in multi-well hydrofracturing;
3. In the quantitative analysis of the length and volume of fracture networks, the total length of hydraulic fractures decreases with the decrease of well spacing, and the total volume of hydraulic fractures increases with the decrease of well spacing. When the well spacing is set to 75 m under the field conditions in this study, a larger total length and volume of fracture propagation can be obtained.

In this paper, the fracture propagation and stress evolution of different well spacings in multi-well hydrofracturing are analyzed and studied. On the other hand, varying the fracturing sequence of multiple wells is actually a form of varying the well spacing. In multi-well hydrofracturing, different initiation sequences of horizontal wells may also affect unstable fracture propagation and the surrounding stress evolution. In future research, it is necessary to study the behaviors and mechanisms of unstable fracture propagation induced by varying the fracturing sequence of multiple wells.

Author Contributions: Y.W., conceptualization, methodology, resources, writing—reviewing and editing, supervision, project administration, funding acquisition. N.L., methodology, software, formal analysis, investigation, data curation, writing—original draft preparation, visualization. All authors have read and agreed to the published version of the manuscript.

Funding: National Natural Science Foundation of China (grants 41877275 and 51608301), Beijing Natural Science Foundation (grant L212016), Yue Qi Young Scholar Project Foundation of China University of Mining and Technology, Beijing (grant 2019QN14), Fundamental Research Funds for the Central Universities, Ministry of Education of China (grant 2019QL02), Teaching Reform and Research Projects of Undergraduate Education of China University of Mining and Technology, Beijing (grants J210613, J200709, and J190701), and the Open Fund of Tianjin Key Lab of Soft Soil Characteristics and Engineering Environment (grant 2017SCEEKL003).

Institutional Review Board Statement: Not applicable.

Informed Consent Statement: Not applicable.

Data Availability Statement: Not applicable.

Acknowledgments: The authors gratefully acknowledge financial support from the National Natural Science Foundation of China (grants 41877275 and 51608301), Beijing Natural Science Foundation (grant L212016), Yue Qi Young Scholar Project Foundation of China University of Mining and Technology, Beijing (grant 2019QN14), Fundamental Research Funds for the Central Universities, Ministry of Education of China (grant 2019QL02), Teaching Reform and Research Projects of Undergraduate Education of China University of Mining and Technology, Beijing (grants J210613, J200709, and J190701) and the Open Fund of Tianjin Key Lab of Soft Soil Characteristics and Engineering Environment (grant 2017SCEEKL003).

Conflicts of Interest: The authors declare no conflict of interest.

References

1. Wang, T.; Tian, S.; Zhang, W.; Ren, W.; Li, G. Production model of a fractured horizontal well in shale gas reservoirs. *Energy Fuels* **2020**, *35*, 493–500. [CrossRef]
2. Olson, J.E.; Taleghani, A.D. Modeling simultaneous growth of multiple hydraulic fractures and their interaction with natural fractures. In Proceedings of the SPE Hydraulic Fracturing Technology Conference, The Woodlands, TX, USA, 19–21 January 2009. [CrossRef]
3. Bunger, A.P.; Jeffrey, R.G.; Kear, J.; Zhang, X.; Morgan, M. Experimental investigation of the interaction among closely spaced hydraulic fractures. In Proceedings of the 45th U.S. Rock Mechanics/Geomechanics Symposium, San Francisco, CA, USA, 26–29 June 2011. [CrossRef]
4. Bunger, A.P.; Zhang, X.; Jeffrey, R.G. Parameters affecting the interaction among closely spaced hydraulic fractures. *SPE J.* **2012**, *17*, 292–306. [CrossRef]

5. He, Q.Y.; Suorineni, F.T.; Ma, T.H.; Oh, J. Effect of discontinuity stress shadows on hydraulic fracture re-orientation. *Int. J. Rock Mech. Min.* **2017**, *91*, 179–194. [CrossRef]
6. Manriquez, A.L. Stress behavior in the near fracture region between adjacent horizontal wells during multistage fracturing using a coupled stress-displacement to hydraulic diffusivity model. *J. Petrol. Sci. Eng.* **2018**, *162*, 822–834. [CrossRef]
7. Noii, N.; Fan, M.; Wick, T.; Jin, Y. A quasi-monolithic phase-field description for orthotropic anisotropic fracture with adaptive mesh refinement and primal–dual active set method. *Eng. Fract. Mech.* **2021**, *258*, 108060. [CrossRef]
8. Xia, L.; Yvonnet, J.; Ghabezloo, S. Phase field modeling of hydraulic fracturing with interfacial damage in highly heterogeneous fluid-saturated porous media. *Eng. Fract. Mech.* **2017**, *186*, 158–180. [CrossRef]
9. Roussel, N.P.; Sharma, M.M. Optimizing fracture spacing and sequencing in horizontal-well fracturing. *SPE Prod. Oper.* **2011**, *26*, 173–184. [CrossRef]
10. Nagel, N.; Zhang, F.; Sanchez-Nagel, M.; Lee, B.; Agharazi, A. Stress shadow evaluations for completion design in unconventional plays. In Proceedings of the SPE Unconventional Resources Conference Canada, Calgary, AB, Canada, 5–7 November 2013. [CrossRef]
11. Manchanda, R.; Sharma, M.M. Impact of completion design on fracture complexity in horizontal shale wells. *SPE Drill. Completion* **2014**, *29*, 78–87. [CrossRef]
12. Wu, K.; Olson, J.E. Simultaneous multifracture treatments: Fully coupled fluid flow and fracture mechanics for horizontal wells. *SPE J.* **2015**, *20*, 337–346. [CrossRef]
13. Bai, T.; Pollard, D.D.; Gao, H. Explanation for fracture spacing in layered materials. *Nature* **2000**, *403*, 753–756. [CrossRef]
14. Warpinski, N.R. Analytic crack solutions for tilt fields around hydraulic fractures. *J. Geophys. Res.-Solid Earth* **2020**, *105*, 23463–23478. [CrossRef]
15. Sobhaniaragh, B.; Mansur, W.J.; Peters, F.C. The role of stress interference in hydraulic fracturing of horizontal wells. *Int. J. Coal Sci. Technol.* **2018**, *106*, 153–164. [CrossRef]
16. Lu, C.; Guo, J.C.; Liu, Y.X.; Yin, J.; Deng, Y.; Lu, Q.L.; Zhao, X. Perforation spacing optimization for multi-stage hydraulic fracturing in Xujiahe formation: A tight sandstone formation in Sichuan Basin of China. *Environ. Earth Sci.* **2015**, *73*, 5843–5854. [CrossRef]
17. Tian, W.; Li, P.; Dong, Y.; Lu, Z.; Lu, D. Numerical simulation of sequential, alternate and modified zipper hydraulic fracturing in horizontal wells using XFEM. *J. Petrol. Sci. Eng.* **2019**, *183*, 106251. [CrossRef]
18. Wang, Y.; Li, X.; Wang, J.B.; Zheng, B.; Zhang, B.; Zhao, Z.H. Numerical modeling of stress shadow effect on hydraulic fracturing. *Nat. Gas Geosci.* **2015**, *26*, 1941–1950.
19. Ghazal, I.; Michael, G.; Leonardo, C.; Christine, B.; Daniel, M.; Fu, P. Fully 3D hydraulic fracturing model: Optimizing sequence fracture stimulation in horizontal wells. In Proceedings of the 49th U.S. Rock Mechanics/Geomechanics Symposium, San Francisco, CA, USA, 28 June–1 July 2015; p. ARMA-2015-119.
20. Kumar, D.; Ghassemi, A. A three-dimensional analysis of simultaneous and sequential fracturing of horizontal wells. *J. Petrol. Sci. Eng.* **2016**, *146*, 1006–1025. [CrossRef]
21. Ju, Y.; Li, Y.; Wang, Y.L.; Yang, Y. Stress shadow effects and microseismic events during hydrofracturing of multiple vertical wells in tight reservoirs: A three-dimensional numerical model. *J. Nat. Gas Sci. Eng.* **2020**, *84*, 103684. [CrossRef]
22. Wong, S.W.; Geilikman, M.; Xu, G. Interaction of multiple hydraulic fractures in horizontal wells. In Proceedings of the SPE Unconventional Gas Conference and Exhibition, Muscat, Oman, 28–30 January 2013. [CrossRef]
23. Segatto, M.; Colombo, I. Use of reservoir simulation to help gas shale reservoir estimation. In Proceedings of the International Petroleum Technology Conference (IPTC'11), Bangkok, Thailand, 15–17 November 2011. [CrossRef]
24. Liu, X.; Rasouli, V.; Guo, T.; Qu, Z.; Sun, Y.; Damjanac, B. Numerical simulation of stress shadow in multiple cluster hydraulic fracturing in horizontal wells based on lattice modelling. *Eng. Fract. Mech.* **2020**, *238*, 107278. [CrossRef]
25. Li, S.; Zhang, D. A fully coupled model for hydraulic-fracture growth during multiwell-fracturing treatments: Enhancing fracture complexity. *SPE Prod. Oper.* **2018**, *33*, 235–250. [CrossRef]
26. He, Y.; Yang, Z.; Li, X.; Song, R. Numerical simulation study on three-dimensional fracture propagation of synchronous fracturing. *Energy Sci. Eng.* **2020**, *8*, 944–958. [CrossRef]
27. Duan, K.; Li, Y.C.; Yang, W.D. Discrete element method simulation of the growth and efficiency of multiple hydraulic fractures simultaneously-induced from two horizontal wells. *Geomech. Geophys. Geo.* **2021**, *7*, 3. [CrossRef]
28. Wu, K.; Wu, B.; Yu, W. Mechanism analysis of well interference in unconventional reservoirs: Insights from fracture-geometry simulation between two horizontal wells. *SPE Prod. Oper.* **2018**, *33*, 12–20. [CrossRef]
29. Jo, H. Optimizing fracture spacing to induce complex fractures in a hydraulically fractured horizontal wellbore. In Proceedings of the SPE Americas Unconventional Resources Conference, Pittsburgh, PA, USA, 5–7 June 2012. [CrossRef]
30. Manchanda, R.; Sharma, M.M. Time-delayed fracturing: A new strategy in multi-stage, multi-well pad fracturing. In Proceedings of the SPE Annual Technical Conference and Exhibition, New Orleans, LA, USA, 30 September–2 October 2013. [CrossRef]
31. Wu, K.; Olson, J.E. Numerical investigation of complex hydraulic-fracture development in naturally fractured reservoirs. *SPE Prod. Oper.* **2016**, *31*, 300–309. [CrossRef]
32. Tsang, C.F.; Stephansson, O.; Hudson, J.A. A discussion of thermos-hydro-mechanical (THM) processes associated with nuclear waste repositories. *Int. J. Rock Mech. Min.* **2000**, *37*, 397–402. [CrossRef]

33. Rutqvist, J.; Barr, D.; Datta, R.; Gens, A.; Millard, A.; Olivella, S.; Tsang, C.F.; Tsang, Y. Coupled thermal–hydrological–mechanical analyses of the Yucca Mountain Drift Scale Test—Comparison of field measurements to predictions of four different numerical models. *Int. J. Rock Mech. Min.* **2005**, *42*, 680–697. [CrossRef]
34. Wang, Y.; Ju, Y.; Chen, J.; Song, J. Adaptive finite element–discrete element analysis for the multistage supercritical CO_2 fracturing and microseismic modelling of horizontal wells in tight reservoirs considering pre-existing fractures and thermal-hydro-mechanical coupling. *J. Nat. Gas Sci. Eng.* **2019**, *61*, 251–269. [CrossRef]
35. Wang, Y.; Ju, Y.; Yang, Y. Adaptive finite element-discrete element analysis for microseismic modelling of hydraulic fracture propagation of perforation in horizontal well considering pre-existing fractures. *Shock Vib.* **2018**, *2018*, 1–14. [CrossRef]
36. Wang, Y.L. Adaptive finite element–discrete element analysis for stratal movement and microseismic behaviours induced by multistage propagation of three-dimensional multiple hydraulic fractures. *Eng. Comput.* **2020**, *38*, 2781–2809. [CrossRef]
37. Wang, Y.L.; Liu, X.G. Stress-dependent unstable dynamic propagation of three-dimensional multiple hydraulic fractures with improved fracturing sequences in heterogeneous reservoirs: Numerical cases study via poroelastic effective medium model. *Energy Fuels* **2021**, *35*, 18543–18562. [CrossRef]
38. Inui, S.; Ishida, T.; Nagaya, Y.; Nara, Y.; Chen, Y.; Chen, Q. AE monitoring of hydraulic fracturing experiments in granite blocks using supercritical CO_2, water and viscous oil. In Proceedings of the 48th U.S. Rock Mechanics/Geomechanics Symposium, Minneapolis, MN, USA, 1–4 June 2014; p. ARMA-2014-7163.
39. Wang, Y.; Ju, Y.; Zhang, H.; Gong, S.; Song, J.; Li, Y.; Chen, J. Adaptive finite element–discrete element analysis for the stress shadow effects and fracture interaction behaviours in three-dimensional multistage hydrofracturing considering varying perforation cluster spaces and fracturing scenarios of horizontal wells. *Rock Mech. Rock Eng.* **2021**, *54*, 1815–1839. [CrossRef]